Modeling the Effects of Oblique Subduction on Mantle Wedge Seismic Anisotropy

Lindsey M. Kenyon and Ikuko Wada
kenyo099@umn.edu, iwada@umn.edu
University of Minnesota Twin Cities Department of Earth Sciences

1. Introduction

This study examines the effect of subduction obliquity on the patterns of mantle flow, olivine CPO, and seismic anisotropy in the mantle wedge. Previous studies have shown that when the subduction direction is oblique to the margin, coupling between the subducting slab and the overriding mantle induces a complex 3-D mantle wedge flow pattern [e.g., Kneller and van Keken, 2008; Wada et al., 2015]. A series of 3-D kinematic-dynamic models for generic subduction systems have been created by varying subduction obliquity. The models show that the directions of trench-ward inflow and down-dip outflow of the mantle in the mantle wedge are both oblique to the margin. For a given mantle flow pattern, we compute the pattern of olivine CPO in the mantle wedge, using the crystallographic code DRex [Kaminski et al., 2004]. We then compute the splitting parameters using the MSAT toolbox [Walker and Wookey 2012]. The resulting fast directions associated with the longest time delays are mostly perpendicular to the margins.

2. Methods

2.1 Temperature and Velocity Model

The finite element code PGCTherm3D is used to model temperature and mantle wedge flow velocity in a generic subduction model setting. A wet olivine dislocation creep rheology is applied to the mantle. We model subduction obliquity for 30°, 45°, and 60° to test its effects.

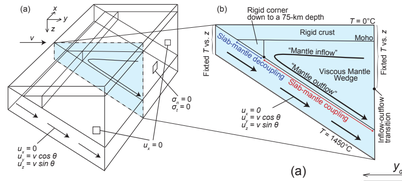

Figure 2.1 Model boundary conditions. The trench side geotherm is calculated by a GDH1 plate-cooling model for a 100 Ma plate [Stein and Stein, 1992] and the back-arc-side geotherm is calculated based on 75mW/m² surface heat flow and the 1350° C mantle potential temperature.

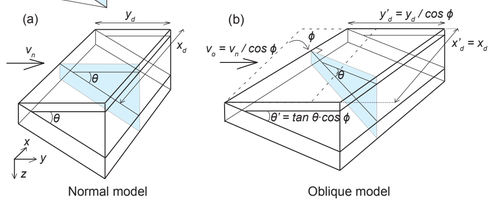

Figure 2.2 Model setup for obliquity. Subduction rate in the downdip direction (Vn) is the same for all models. The subduction direction is due east in all models.

Governing Equations

The code solves the equations of conservation of mass (1), momentum (2) and heat equation (3). The effect of shear heating is excluded.

$$\nabla \cdot \mathbf{v} = 0 \quad (1)$$

$$\nabla \cdot \sigma' - \nabla P = 0 \quad (2)$$

$$\nabla \cdot (k\nabla T) - \rho c_p (\mathbf{v} \cdot \nabla T) + Q_H = 0 \quad (3)$$

v is the flow velocity, σ´ is the deviatoric stress tensor, P is dynamic pressure generated by mantle flow, k is thermal conductivity, T is temperature, ρ is density, cp is specific heat, and Q_H is the volumetric heat production which includes radiogenic heat production only.

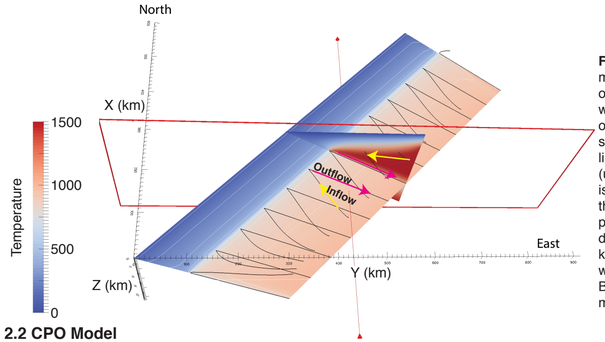

Figure 2.3 Calculated mantle flow stream lines for our subduction zone model with 45° slab dip and 45° obliquity. The slab surface is shown below the stream lines. The cross section (used for results in section 3) is taken at the mid-point of the model (red box) and is parallel to the subduction direction. The model is 600 km long in the X direction which minimizes the effect of BCs in the central part of the model.

2.2 CPO Model

The fast axis is modeled using DRex [Kaminski et al., 2004] for an A-type fabric. DRex depends on the nucleation parameter (λ), the threshold volume for grain boundary sliding (χ), and the grain boundary sliding mobility (M). Values are λ = 5, χ = 0.3, and M=125 [Boneh et al., 2015, Faccenda and Capitanio, 2013] for all models. Cross sections for DRex calculation are taken parallel to the convergence direction (Y-axis). The deformation history for all models is limited to 5 million years.

3. Results

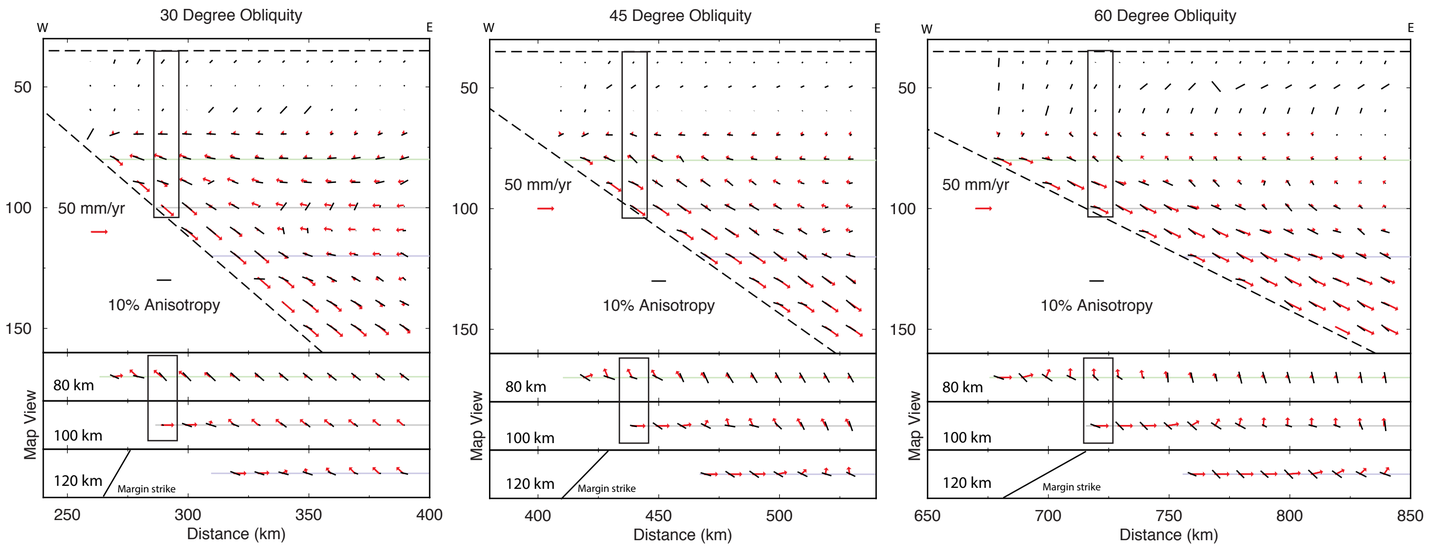

Figure 3.1 Velocity (red arrows) and average fast axis orientation (black bars) in cross-section (top panel) and in map view (bottom three panels) at three different depths 80km, 100km and 120km for models with 30°, 45° and 60° obliquity. The rectangles inside the plots indicate the location of the tensors used for Figure 3.2.

3.1 Velocity Model and Fast Axis Orientation

The direction of the mantle flow toward the mantle wedge corner at depths of 70km to 90km is dependent on the amount of obliquity in the model, but is generally oriented in a NW to N direction. Looking right to left at a depth slice in map view, the mantle flow velocity azimuth rotates clockwise from NW-N (inflow) to due east (outflow). The average fast azimuth for the inflow area is nearly parallel to the flow direction in all models. Where the flow transitions from inflow to outflow, the average fast azimuth is oriented closer to E-W, perpendicular to the flow. In the entrained down-going mantle the angle between the mantle wedge outflow and the average fast axis azimuth increases with increased obliquity.

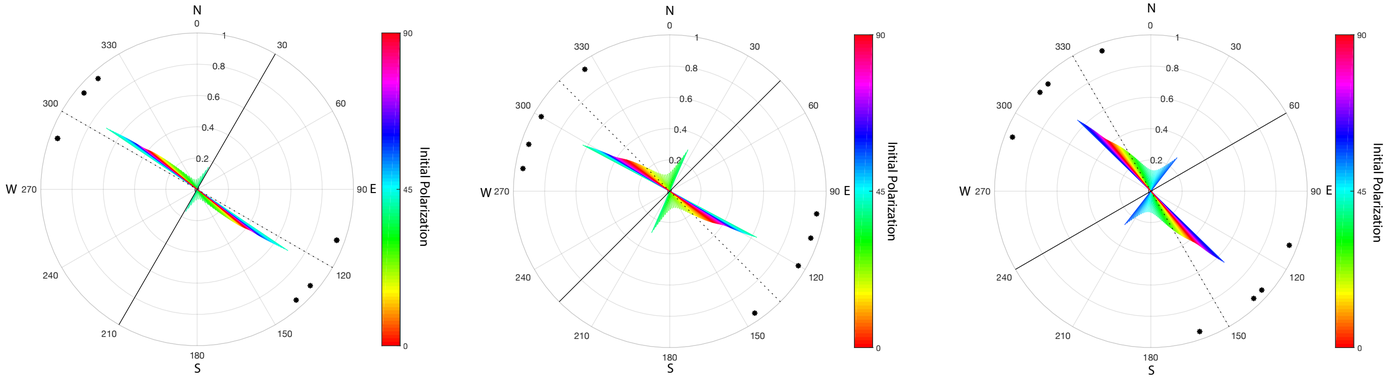

Figure 3.2 The effective fast direction (orientation of the plotted bars), and effective time delay (the length of the bar) of the sub-arc mantle wedge. The parameters are dependent on the initial polarization and have a 90° periodicity, thus initial polarization values are only plotted for values ranging from 0° to 90° (see color bar) The incidence angle of the seismic wave is vertical. The black dots indicate the fast azimuth of the individual layers. The black solid line on the plot indicates the margin orientation and the dashed black line indicates the margin perpendicular direction.

3.2 Splitting Parameters

The fast azimuth with the longest time delays (~0.7 sec) for all models is SE or ~120°, but varies with initial polarization and all plots show a smaller (~0.3 sec) time delay peak to the NE at ~30°. Qualitatively, the majority of the fast azimuths with the longest time delays are sub-normal to the margin (within ~20° of perpendicular). All plots show a large dependence on initial polarization for both splitting parameters, yet have generally similar results despite the changes in obliquity.

4. Next Steps

The consistent margin perpendicular fast azimuths for all obliquity models is surprising provided the variation in mantle wedge flow directions for changes in obliquity. The next steps in this work is to consider other olivine fabric types and more complex margin geometries.

5. References

Boneh, Y., Morales, L. F. G., Kaminski, E., & Skemer, P. (2015). Modeling olivine CPO evolution with complex deformation histories: Implications for the interpretation of seismic anisotropy in the mantle. Geochemistry, Geophysics, Geosystems, 16(10), 3436–3455. https://-doi.org/10.1002/2015GC005964

Faccenda, M., & Capitanio, F. A. (2013). Seismic anisotropy around subduction zones: Insights from three-dimensional modeling of upper mantle deformation and SKS splitting calculations. Geochemistry, Geophysics, Geosystems, 14(1), 243–262. https://-doi.org/10.1002/ggge.20055

Kaminski, E., Ribe, N. M., & Browaeys, J. T. (2004). D-Rex, a program for calculation of seismic anisotropy due to crystal lattice prefferred orientation in the convective upper mantle. Geophysical Journal International, 158(2), 744–752. https://-doi.org/10.1111/j.1365-246X.2004.02308.x

Kneller, E. A., & van Keken, P. E. (2008). Effect of three-dimensional slab geometry on deformation in the mantle wedge: Implications for shear wave anisotropy. Geochemistry, Geophysics, Geosystems, 9(1), 1–21. https://-doi.org/10.1029/2007GC001677

Stein, C. A., & Stein, S. (1992). A model for the global variation in oceanic depth and heat flow with lithospheric age. Nature, 359(6391), 123–129. https://-doi.org/10.1038/359123a0

Wada, I., He, J., Hasegawa, A., & Nakajima, J. (2015). Mantle wedge flow pattern and thermal structure in Northeast Japan: Effects of oblique subduction and 3-D slab geometry. Earth and Planetary Science Letters, 426, 76–88. https://-doi.org/10.1016/j.epsl.2015.06.021

Walker, A. M., & Wookey, J. (2012). MSAT-A new toolkit for the analysis of elastic and seismic anisotropy. Computers and Geosciences, 49, 81–90. https://-doi.org/10.1016/j.cageo.2012.05.031